Radio meteors

Visualizing meteor streams by radio forward scattering on the basis of meteor head echoes

Wolfgang Kaufmann[1]

The outcome of radio meteor observation of a basic monitoring system based on forward scattering can be enhanced by additionally analysing meteor head echoes. Meteoroids of common origin produce in a circumscribed area of reflection a bunch of head echoes with equally Doppler shifted frequency gradients. These can be made visible in a kernel density map. Measurements are performed to verify this idea and to outline the possibilities and constraints. The described method proves to provide a spatially differentiated depiction of the monitored meteoric activity.

Received 2018 January 15

1 Introduction

The observation of radio meteors via forward scattering can be performed 24h a day regardless of clouds and the position of the sun and the moon. As long as only the presence of a meteor will be detected this will not provide any positional information about it. This is a severe shortcoming of forward scattering. To overcome this at least an interferometric system must be built up (Rendtel & Arlt, 2015). In this paper a new way for a basic radio monitoring station is described to identify different origins of meteors. It requires a radio meteor receiving and detecting system that is able to pick up meteor head echoes and their frequency change with a sufficient time and frequency resolution.

Meteor head echoes are radio waves scattered from the small intense plasma region surrounding the meteoroid during its atmospheric passage. On its flight a meteoroid shows a permanent changing radial velocity with respect to the observer (Kero et al., 2008). Also it undergoes a deceleration dependent on its physical characteristics and entry velocity (Kikwaya et al., 2009). So Doppler shift of the reflected radio frequency is not constant but reveals a specific slope. Meteoroids of a shower move on almost parallel trajectories and their head echoes should produce a consistent group of frequency slopes in a circumscribed region of reflection. These groups can be made visible in a kernel density plot. So, different sources of meteoric activity in the sky can be detected. Yet a localisation of the radiant cannot be achieved by this procedure. This is out of the reach of a single basic forward scattering system.

The practical procedure and the results of four observation sessions are described and shall demonstrate the possibilities of forward scattering taking in account head echoes.

2 Material and Methods

The French radar-transmitter GRAVES was employed for forward scattering. It transmits a continuous rf-signal at a frequency of 143.050 MHz and illuminates a well defined region of the sky in 100 km height, see Figure 1. Receiving location was Algermissen, Northern Germany (N 52°15′16, E 009°58′71). A HB9CV-antenna was directed to the transmitter location and fed to a FUNcube Dongle Pro+ (FCDP). The FCDP is a software defined receiver.[a] This means all filtering and demodulation is done by software. SDR# was used as receiving software.[b] It was set to USB, 143.049 MHz receiving frequency, 48 kHz audio output, audio filtering and AGC switched off. The audio output was fed to the software Meteor Logger[c], which detects and logs meteor signals within an audio stream (Kaufmann, 2017). It reveals a continuous output i.a. of the frequency of the detected signal in 10.7 ms steps. Both programs ran on the same computer (Intel i5, clock speed 2.3 GHz) with Windows 7.

For post processing of the gathered data, the software Process Data[c] was used to reduce interference and extract the frequency slopes of the received head echoes. First the software calculates the median of all recorded frequencies, $f(\text{median})$, gradually to take account of a possible receiver drift. Hereby $f(\text{median})$ represents the frequency of the meteor trails because these are much more numerous than head echoes. Then the software reduces interference by eliminating any signal that do not contain at least one frequency in the range of $f(\text{median}) \pm 2df$, where df is the frequency resolution of the measurement (it is predefined by Meteor Logger to 23.4 Hz). At least the software runs through the frequencies, $f(i)$, of each signal and checks for the following three conditions that must be fulfilled cumulative to identify an analysable head echo, see Figure 2, upper graph:

1. start frequency $f(i = 1)$ must be $\geq 5df + f(\text{median})$,
2. each subsequent frequency, $f(i + 1)$, must be $\leq$ its precedent frequency, $f(i)$ until $f(i) < 2df + f(\text{median})$,
3. number of frequencies, fulfilling (1) and (2), must be ≥ 3.

[1]Lindenweg 1e, 31191 Algermissen, Germany.
Email: contact@ars-electromagnetica.de

IMO bibcode WGN-461-kaufmann-radio
NASA-ADS bibcode 2018JIMO...46...39K

[a]http://www.funcubedongle.com/
[b]https://airspy.com/download/
[c]http://www.ars-electromagnetica.de/robs/download.html

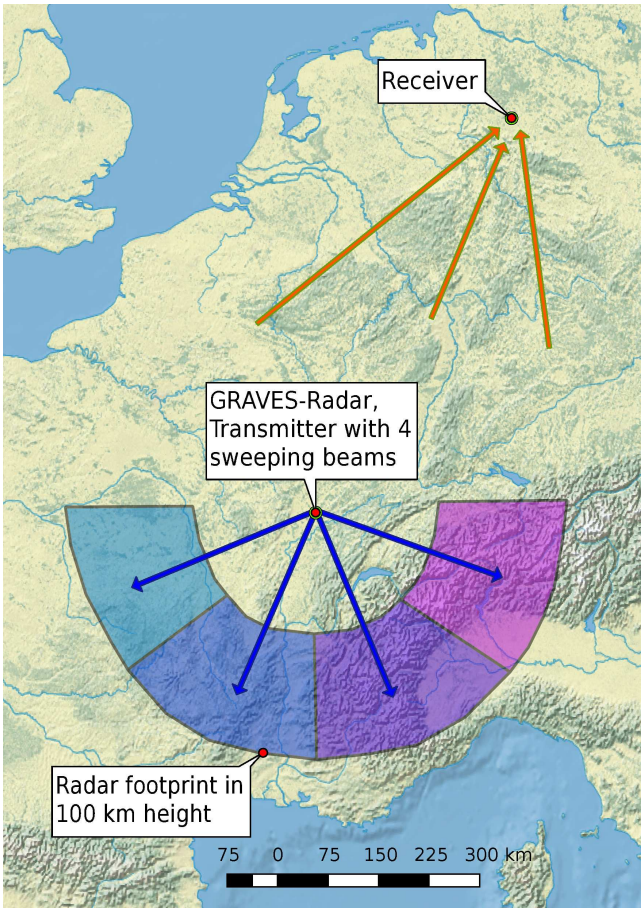

Figure 1 – Footprint of the French GRAVES radar and location of the receiver at Northern Germany. Four radar beams continuously sweep in steps of 7.5° each 0.8 s in azimuthal sectors of 45°.[d] Please note the quoted paper still states steps of 3.2 s duration, this has been changed a few years ago to 0.8 s. Map made with Natural Earth.

From the resulting time series of frequencies of a head echo signal the slope was calculated by the software by means of a linear regression analysis.

The extracted frequency slopes with associated date-time stamps were transformed to obtain the same scale. The date-time stamp was converted to a decimal number, starting from the first day of detection at 00^h UTC with 0.0. To the absolute value of the frequency slope a decadic logarithm was applied to reduce the skewness of the distribution. Finally by means of the statistic software PAST (Hammer et al., 2001)[e], a kernel density map was produced with these pairs of data. Thereby a triangular kernel function was selected. This function was found to produce the most structured display. For a better readability the decimal day indication was replaced by date-time markers in the finished plot.

For comparative purposes also the hourly count rates (HCR) of all registered meteor-signals are determined. This again was obtained with the software Process Data. After reduction of interference the remaining signals were conflated if the time span between two signals was less than 0.525 s. If the precedent signal showed a logarithmic decline or the subsequent signal started with a head echo no conflation was performed. Then the number of signals per hour were ascertained and smoothed by a moving average. The resulting bar chart was superimposed on the kernel density map. The hypothetical hourly count rate of sporadic meteors was calculated from a fitted sine function (Powell, 2017) and is also indicated in the bar chart.

The calculation of the altitude of an assumed radiant for each date-time stamp of a received meteor signal was also carried out by Process Data. Right ascension and declination of each radiant was taken from Rendtel (2016). After unity-based normalisation the graph of the altitude was also superimposed on the kernel density map.

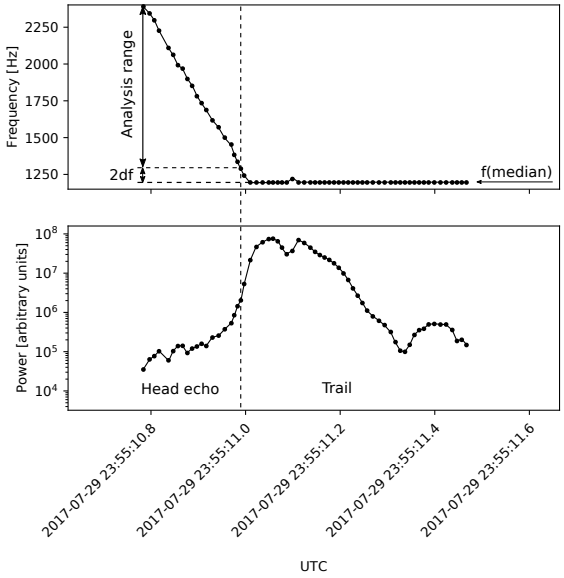

Figure 2 – An example of a meteor signal consisting of head echo and trail. The upper graph shows the progress of the reflected peak frequency. Head echoes are analysed only within the indicated range, for details see text. The lower graph exhibits the corresponding received power.

3 Results

Four radio meteor logging sessions were performed, see Table 1. From all detected meteor signals only about 12% show a head echo. According to Close et al. (2002) the plasma sheet around the meteoroid itself can be assumed to be spherical. Therefore a reflection of a small portion of the incident rf-power in direction of the receiver location should be possible independent of the angle of irradiance. Yet the benefit of the resulting general visibility is counteracted by the low radar cross section (RCS) of small meteoroids. E.g. Close et al. (2002) found a maximum RCS of 0.14 m^2 at 160 MHz for the Leonids. The reflected power at meteor trails is by orders of magnitude higher, see e.g. Figure 2. So smaller or very slow meteoroids can be detected only via their trail whereas their head echoes are too weak to be registered.

Hence the number of observed head echoes mainly depend on the overall sensitivity of the receiving system, the flux density and mass distribution of the me-

[d] http://www.itr-datanet.com/~pe1itr/pdf/The%20143.050MHz%20Graves%20Radar%20a%20VHF%20Beacon.pdf

[e] http://folk.uio.no/ohammer/past/

Table 1 – Brief overview of the radio meteor logging sessions.

Main Meteor Shower	Date and Time [UTC] of Observation 2017	Number of Detected Meteors	Number of Detected Head Echoes	Percentage of Head Echoes
SDA	Jul 27 03^h00^m – Jul 31 19^h59^m	8267	990	12.0%
PER	Aug 09 20^h00^m – Aug 14 17^h59^m	11663	1226	10.5%
DSX	Sep 25 03^h00^m – Sep 29 16^h59^m	6251	804	12.9%
ORI	Oct 18 20^h00^m – Oct 23 17^h59^m	8015	1090	13.6%

teor stream (Belkovich et al., 2005) and analogously to Lambert's cosine law to the angle of incidence. However the frequency slope of a head echo depends on the velocity and trajectory of its decelerating meteoroid in relation to both the transmitter position as well as the receiver position. In a kernel density map both the number and the frequency slopes of all observed head echoes can be combined: numerous head echoes with similar frequency slopes will be apparent as hot spots.

In the following the specific logging sessions will be addressed by their present main meteor shower according to Table 1. To interpret the findings in the kernel density maps the progress of the Zenithal Hourly Rate (ZHR) of a meteor stream was taken from Rendtel (2014). The active showers at a given time span were extracted from Rendtel (2016).

3.1 The Perseids (PER) observation

The PER are known to show high ZHR during their broad maximum. This minimizes the influence of all other sources of meteors. The radiant of PER circled well above the horizon in the northern sky which was basically true for the complete time span of the observations, see Figure 3, top. As can be seen in Figure 4 from about August 12 03^h to August 14 10^h UTC there was a strong presence of head echoes with common frequency slopes. With the diurnal movement of the radiant in terms of altitude and azimuth also the trajectories of the meteoroids changed relative to transmitter and receiver. This led to an altered progress of the radial velocities resulting in a serrated sequence of diurnal changing values of the frequency slopes as indicated in Figure 4. This pattern recurs in the azimuthal course of the radiant with daytime, see Figure 3, bottom. Between 02^h and 09^h UTC there was a fast change from East to West whereas the return to East was much slower.

The density of the slopes of the head echoes along the track of PER showed to be variable. In principle it followed the overall meteor shower activity as can be derived from the difference between observed HCR and the assumed amount of the sporadic meteors. In detail there were some deviations. E.g. the maximum of HCR on August 13 05^h UTC did not produce the highest density in the plot. Also the steep rise of the track on August 12 from about $04^h - 08^h$ UTC did not recur such pronounced on August 13 and 14 despite similar or higher HCR. So variations in the mass distribution also may contribute.

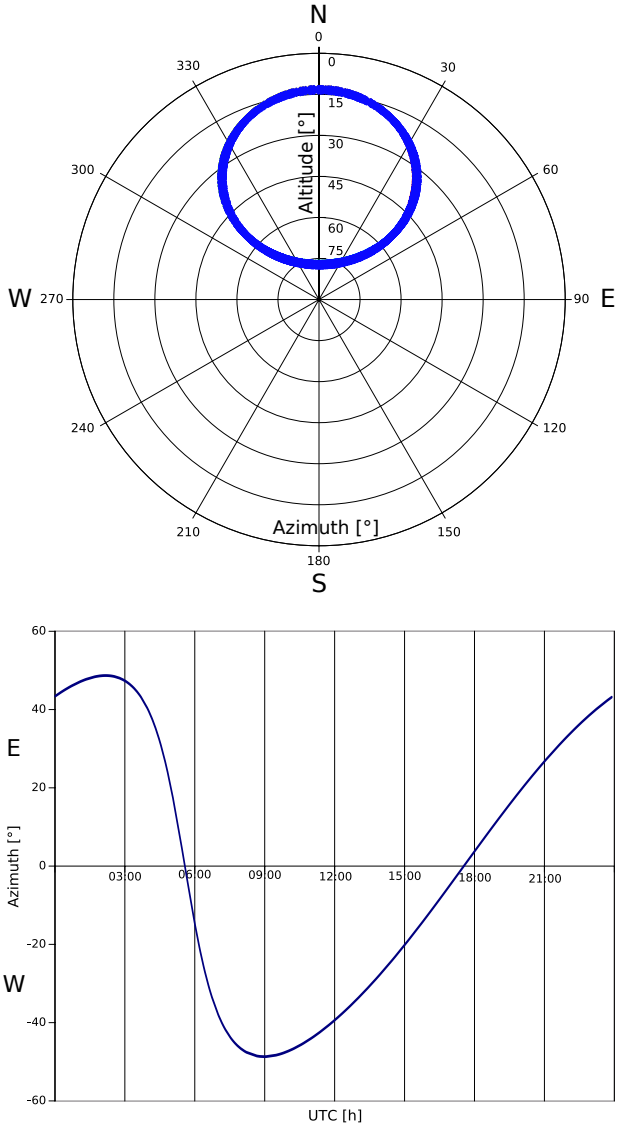

Figure 3 – Top: Polar plot of altitude and azimuth of the radiant of PER at the location of the footprint of GRAVES on August 12. Bottom: Plot of the azimuth of the radiant of PER against daytime at the location of the footprint of GRAVES on August 12.

3.2 The Southern δ-Aquariids (SDA) observation

Unfortunately there was a high level of noise present from July 28, 22^h UTC to 29, 12^h UTC and again from July 29, 22^h UTC to 30, 17^h UTC. As a consequence the weaker signals were buried resulting in a drastically declined number of observed meteors. So observations

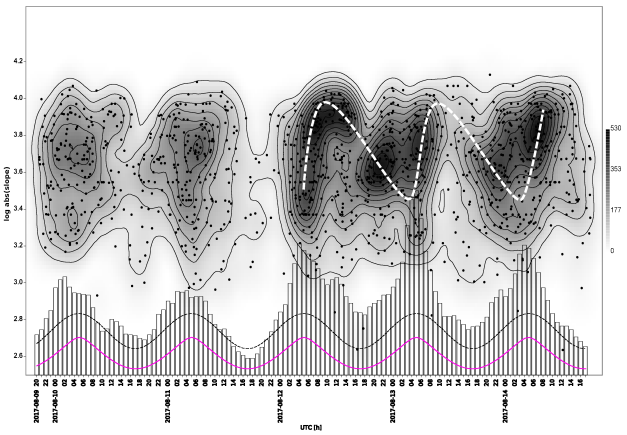

Figure 4 – The PER kernel density map. Each dot represents the frequency slope of a head echo. The dashed line track the PER. Superimposed are the hourly count rates of all observed meteors (min = 23, max = 251 counts/h). Herein the hypothetical amount of sporadic meteors is denoted. Also the normalised altitude of the radiant of the PER is indicated (magenta line) at the location of the footprint of GRAVES radar.

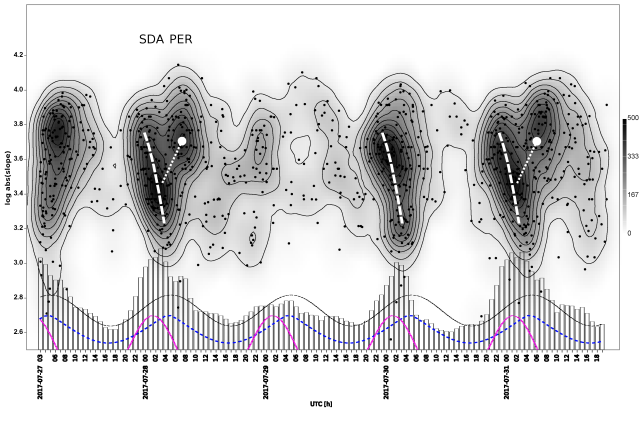

Figure 5 – The SDA kernel density map. Each dot represents the frequency slope of a head echo. Dashed lines track the SDA. Dotted lines simply indicate relations. Superimposed are the hourly count rates of all observed meteors (min = 27, max = 155 counts/h). Herein the hypothetical amount of sporadic meteors is denoted. Also the normalised altitude of the radiants of the SDA (magenta) and PER (blue) are indicated at the location of the footprint of GRAVES radar.

on July 29 turn out to be a complete failure and were strongly biased on July 30.

Together with the predominant SDA at least PAU, CAP and PER should be present during the observation. The diurnal changing values of the frequency slopes of the SDA can be tracked in the kernel density map at least on July 28 and 31, see Figure 5. PAU and CAP cannot be identified individually because of their low flux densities in combination with their high proximity to the radiant of SDA. All three radiants only temporarily moved above the horizon for a restricted range of azimuth. This depicts as a short track of changing values of the frequency slopes of the common head echoes. However the PER are well distinguishable. Their frequency slopes form a single hot spot when their radiant was near its maximum altitude. Outside the maximum altitude the number of observed head echoes was too low to be mapped. The curve of HCR shows the SDA as high peak and the PER as tiny subsidiary summit.

3.3 The Orionids (ORI) observation

During this observation besides the predominant ORI also the EGE and LMI were active. The ORI produced much smaller HCR than the SDA so the sporadic meteor background cannot be neglected anymore. At least the antihelion source with mainly the STA/NTA and the helion source should be considered. The radiants of all above-mentioned sources only temporarily rose above the horizon. The ORI exhibit diurnal changing values of the frequency slopes in form of short tracks in the kernel density map, see Figure 6. ORI and EGE cannot be identified individually because of the low activity of EGE in combination with the fairly adjacent radiants of the two streams. The STA/NTA and LMI/helion source can be recognised as ellipsoids very clearly on October 20 but can be found also during the other days of the observation. STA/NTA, ORI and

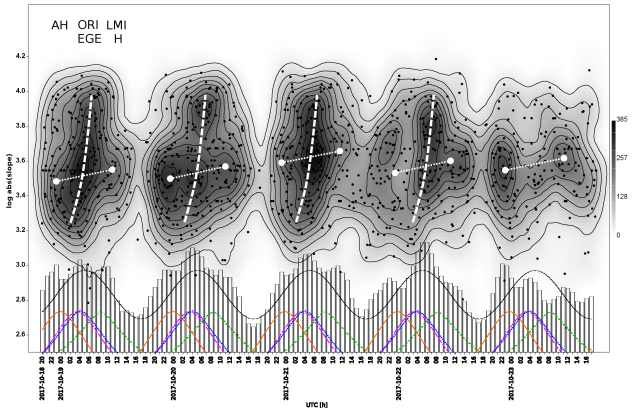

Figure 6 – The ORI kernel density map. Each dot represents the frequency slope of a head echo. Dashed lines track the ORI. Dotted lines simply indicate relations. Superimposed are the hourly count rates of all observed meteors (min = 25, max = 108 counts/h). Herein the hypothetical amount of sporadic meteors is denoted. Also the normalised altitude of the radiants of the antihelion source AH (on base of the radiants of the NTA/STA, orange), the ORI (magenta), EGE (blue) and LMI (green) are indicated at the location of the footprint of GRAVES radar (from left to right). H = helion source.

LMI/helion source also are visible in the curve of the HCR as separate peaks or shoulders.

The density distribution of the frequency slopes of the head echoes along the diurnal tracks of the ORI noticeably differed from one day to the next. Especially on October 20 and 22 the overall density was low despite a high value of HCR. A noticeable change in the mass distribution towards lower number of meteoroids with higher masses may be assumed.

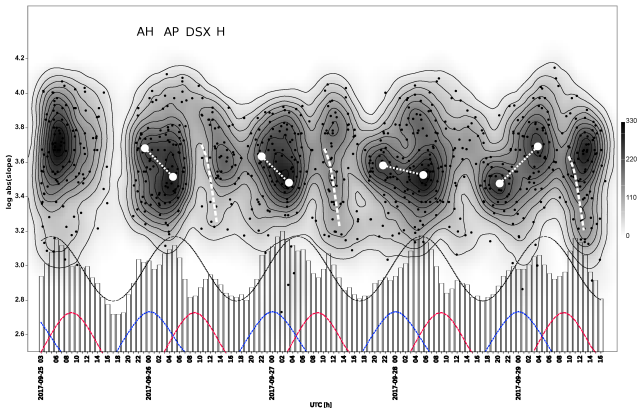

Figure 7 – The DSX kernel density map. Each dot represents the frequency slope of a head echo. Dashed lines track the DSX. Dotted lines simply indicate relations. Superimposed are the hourly count rates of all observed meteors (min = 27, max = 86 counts/h). Herein the hypothetical amount of sporadic meteors is denoted. Also the normalised altitude of the radiants of the antihelion source AH (on base of the radiants of the STA, blue) and the DSX (red) are indicated at the location of the footprint of GRAVES radar (from left to right). AP = apex source, H = helion source.

3.4 The Daytime Sextantids (DSX) observation

Within the observation period, the minor active DSX and from the sporadic meteor background the helion source, the apex source and the antihelion source with mainly the STA were present. Their radiants rose only temporarily above the horizon. Sporadic meteors dominated the hourly count rates, see Figure 7. The prominent diurnal hot spots at 05^{h} UTC (= 06^{h} local time) in the kernel density map coincided with the maximum activity of the apex source (Rendtel, 2006). The diurnal short tracks of changing values of the frequency slopes of the DSX onto the background of the helion source can be assumed on September 26, 27 and 29. On September 28 only the HCR show a small peak at 12^{h} UTC, a clear representation in the kernel density map cannot be found. The antihelion source can be well distinguished from the apex source both being depicted as ellipsoids. Yet the density centres of both change their positions relative to each other to a great degree. Both sources cannot be distinguished reliably in the curve of HCR.

4 Discussion

The footprint of GRAVES radar in 100 km height consists of four different fields, see Figure 1. So four different geometrical conditions of reflections exist simultaneously. Hence a meteor stream must be expected to produce four contiguous groups of head echo frequency slopes at the receiver site. This may explain the broadened tracks of the meteor streams as shown in Figures 4–7. This effect reduces the directional sensitivity of the receiving system.

The PER observation validates the theoretical considerations by demonstrating the grouping of head echoes with common frequency slopes originating from a common source. Also a first impression of the variance of the frequency slopes is achieved resulting from different radiant positions. Thereby the azimuth of the radiant has a much greater influence on the resulting radial velocities than the altitude in this observation. This analysis shows that indeed different radiant-positions can be identified via the frequency slopes of head echoes.

The SDA, ORI and DSX observations follow a descending order of radio activity level as described in Ogawa & Steyaert (2017). So, the interaction of meteor shower and sporadic meteors can be gradually studied. The SDA show HCR being well above the sporadic meteor background. Hence only the SDA and the PER appear in the kernel density map. The HCR of ORI exceed the assumed amount of the sporadic meteors only by a small quantity. The antihelion source now becomes apparent in the kernel density map whereas the apex source is widely masked by the ORI. The DSX are almost embedded in the sporadic meteor background. The antihelion and apex source now are visible together with the DSX. Thereby the apex source shows to have higher HCR and higher densities in the kernel density map than the antihelion source. This is in accordance with Jakšová et al. (2015). This analysis shows that the detectability of meteor sources by means of a kernel density map is determined by the activity of the single present streams.

The density within a kernel density map depends on the number of head echoes with similar frequency slopes. This number is a result of mainly (1) the activity of the meteor stream, (2) the altitude of its radiant and (3) its mass distribution. In general the calculated densities are found to follow the difference between observed HCR and the assumed amount of the sporadic meteors, i.e. are primarily characterised by (1) and (2). For the most part the influence of (3) cannot be directly observed. The described inconsistencies between density and HCR being apparent in the kernel density maps of PER and ORI could indicate the impact of (3).

The DSX observation shows an interesting dynamics of the antihelion and apex source of sporadic meteors. Shape and position of highest density vary strongly from day to day in the kernel density map. It can be assumed that this is an expression of the high inhomogeneity of these sources.

5 Conclusion

The density mapping of frequency slopes of head echoes allow a new and more detailed insight in the occurrence of radio meteors received by a basic radio monitoring station. It can help to understand and interpret the course of the observed HCR: individual HCR-segments can be assigned to meteor streams or delimited from various sources of sporadic meteor background and possibly also from interference. Meteor streams with low activity being numerically embedded in the sporadic meteor background can be made visible. The dynamics of various sources of meteors become apparent. So far the presented results are analysed under a qualitative aspect. Further research may show whether quantitative results can also be compiled.

References

Belkovich O. I., Nedeljković S., and Verbeeck C. (2005). "Forward scatter meteor observations". In Verbeeck C. and Wislez J.-M., editors, *Proceedings of the Radio Meteor School, Oostmalle, Belgium, September 10-14, 2005*. International Meteor Organization, pages 55–66.

Close S., Oppenheim M., Hunt S., and Dryud L. (2002). "Scattering characteristics of high-resolution meteor head echoes detected at multiple frequencies". *J. Geophs. Res.*, **107:A10**. SIA 9 (1-12).

Hammer Ø., Harper D. A. T., and Ryan P. D. (2001). "PAST: Paleontological statistics software package for education and data analysis". *Palaeontologia Electronica*, **4:1**, 9pp.

Jakšová I., Porubčan V., and Klačka J. (2015). "Structure and sources of the sporadic meteor background from video observations". *Publ. Astron. Soc. Japan*, **67:5**. (1-7).

Kaufmann W. (2017). "New radio meteor detecting and logging software". *WGN, Journal of the IMO*, **45:4**, 67–72.

Kero J., Szasz C., Pellinen-Wannberg A., Wannberg G., Westman A., and Meisel D. D. (2008). "Determination of meteoroid physical properties from tristatic radar observations". *Ann. Geophys.*, pages 2217–2228.

Kikwaya J.-B., Campbell-Brown M., G. B. P., Hawkes R. L., and Weryk R. J. (2009). "Physical characteristics of very small meteoroids". *A&A*, **497**, 851–867.

Ogawa H. and Steyaert C. (2017). "Major and daytime meteor showers using global radio meteor observations covering the period 2001-2016". *WGN, Journal of the IMO*, **45:5**, 98–106.

Powell C. (2017). "Modelling & analysis of diurnal variation in meteor flux". *WGN, Journal of the IMO*, **45:2**, 32–37.

Rendtel J. (2006). "Sporadic meteors". In Kac J. and Bettonvil F., editors, *Proceedings of the International Meteor Conference, Roden, The Netherlands, September 14-17, 2006*. International Meteor Organization.

Rendtel J., editor (2014). *Meteor Shower Workbook 2014*. International Meteor Organization, Potsdam.

Rendtel J. (2016). "2017 Meteor Shower Calendar". IMO_INFO (2-16).

Rendtel J. and Arlt R. (2015). *Handbook for Meteor Observers*. International Meteor Organization, Potsdam.

Handling Editor: Jean-Louis Rault